Icarus **137**, 235–246 (1999)
Article ID icar.1998.6035, available online at http://www.idealibrary.com on IDEAL®

A Model of Spectral Albedo of Particulate Surfaces: Implications for Optical Properties of the Moon

Yurij Shkuratov and Larissa Starukhina

Astronomical Observatory, Kharkov State University, Sumskaya St., 35, Kharkov, 310022, Ukraine
E-mail: shkuratov@ygs.kharkov.ua

and

Harald Hoffmann and Gabriele Arnold

Institute of Planetary Exploration, German Aerospace Center (DLR), Rudower Chaussee 5, D-12489 Berlin, Germany

Received September 9, 1997; revised June 29, 1998

A simple one-dimensional geometrical-optics model for spectral albedo of powdered surfaces, in particular of lunar regolith, is presented. As distinct from, e.g., the Kubelka–Munk formula, which deals with two effective parameters of a medium, the suggested model uses spectra of optical constants of the medium materials. Besides, our model is invertible, i.e., allows estimations of spectral absorption using albedo spectrum, if *a priori* data on the real part of refractive index and surface porosity are known. The model has been applied to interpret optical properties of the Moon. In particular, it has been shown that: (1) both color indices and depth of absorption bands for regolith-like surfaces depend on particle size, which should be taken into account when correlations between these optical characteristics and abundance of Fe and Ti in the lunar regolith are studied; (2) fine-grained reduced iron occurring in regolith particles affects band minima positions in reflectance spectra of lunar pyroxenes and, consequently, affects the result of determination of pyroxene types and Fe abundance by Adams' method.

INTRODUCTION

To interpret optical data on atmosphereless celestial bodies, models of light scattering by regolithic media are needed. Regoliths of lunar and planetary surfaces have a complicated particulate structure including semitransparent and optically inhomogeneous fragments and aggregates of rocks (minerals) and glasses of different sizes, from submicrometer to millimeter scales. At larger scales, the planetary surfaces have a stochastic relief. Mathematical description of such objects faces huge difficulties and, therefore, a more or less strict theory of light scattering for these objects has not been proposed yet. It may be expected that this theory should be very cumbersome and should operate with many parameters. Even in the geometrical-optics approximation, the problems remain very difficult. At present there are two photometrical models close to each other that describe observational data in first approximation (Hapke 1981, 1986, Lumme and Bowell 1981a,b). The theories operate only five parameters, but even this number is often too much, since they give ambiguous fittings to experimental data (Domingue and Hapke 1989). There is a "vicious circle": the more parameters, the more exact the theory, but the more ambiguous the fits to measured data. Therefore, heuristic models with small numbers of parameters, but giving good fit to observations, seem to be very attractive.

The main purpose of this paper is to propose a simple model of such a kind that describes spectral behavior of albedo of regolith-like surfaces. Our model is based on geometrical-optics approximation. It has an important advantage—it is analytically invertible, i.e., the wavelength behavior of average absorption coefficient of regolith material can be estimated from spectral albedo data. Prototype elements of the model can be found in the works by Stokes (1904), Bodo (1951), Melamed (1963), Hapke (1981), Shkuratov (1982, 1987), Hiroi and Pieters (1992), and Starukhina and Shkuratov (1996).

Spectroscopy of celestial bodies can be considered as a particular case of spectroscopy of a light-scattering object. According to Rosenberg (1967), a general scheme of spectroanalytic experiment includes the following stages: (1) measurement of optical characteristics (e.g., albedo) of the object as a function of wavelength, (2) determination of optical parameters of its light-scattering slab (e.g., volume coefficients of scattering and absorption on the base of the radiation transfer theory), (3) determination of the optical characteristics of an "average" light-scattering element, (4) calculations of the optical constants of the surface material, (5) determination of physical and chemical properties.

Solid surfaces of celestial bodies are objects with chaotic structure. The surface particles display a wide variety of physical properties. Therefore, the scheme cannot be entirely applied

0019-1035/99 $30.00

to these surfaces. The usual approach is to find relationships between spectral and chemical/mineralogical parameters using laboratory measurements of analogs (in the case of the Moon, soil) of celestial bodies surface material. Thus, from the first stage of the spectroanalytic experiment a step is made directly to the last one.

This approach is rather fruitful. For example, the widely known Adams (1974) pyroxene curve presents the relationship between the type of pyroxene and position of the center of the d–d absorption bands formed by Fe^{2+} ions in the ranges near 1 and 2 μm; the "titanium" curve enables one to estimate TiO_2 abundance in mature mare soils of the Moon using measurements of color index C(0.42/0.55 μm) (Charette *et al.* 1974). However, the empirical approach is useful only as a first step. The relationships between spectral and mineralogical parameters should be explained and the limitations of their applications should be found. This requires a completion of all (or the most of) stages in Rosenberg's scheme, at least in a simplified form.

This scheme is partially realized in the models mentioned above (Hapke 1981, 1984, 1986, Lumme and Bowell, 1981a,b). They use the radiation transfer theory to calculate the contribution of multiple scattering. However, as noted in Simons (1975), the theory is effective to estimate average optical characteristics of the medium and not of the material constituting the particles. Determination of the material parameters coming from the optical characteristics of the scattering medium is not a trivial problem. Moreover, the classical radiation transfer scheme cannot be consequently applied to regolithic surfaces. Indeed, the transfer equation uses a small elementary volume of the scattering medium. The volume should include a number of scatterers great enough, but this assumption is correct only for powdered surfaces with rather high albedo.

Often an "average" particle is considered (Hapke 1981) as an elementary volume of particulate medium. The elementary volume is characterized by the albedo of single scattering. To estimate this albedo in the geometrical-optics approximation, an approach based on a one-dimensional model of light scattering was used by some authors, e.g., Melamed (1963), Hapke (1981), and Shkuratov (1982, 1987). In this model multiple reflections in a particle are considered as multiple scattering in a one-dimensional medium with some "effective" reflection coefficients which are the result of averaging the usual Fresnel coefficients over incidence angle.

The main idea of our model is to apply the approach used for single-particle-scattering albedo (Melamed 1963, Hapke 1981, Shkuratov 1982, 1987) to the albedo of a particulate surface (Bodo 1951, Shkuratov 1982, 1987, Starukhina and Shkuratov 1996). We suggest changing scattering in a system of particles (Fig. 1a) to scattering in an equivalent system of plates (Fig. 1b). Thus, we ignore all angle dependences of reflectance, assuming that the calculated one-dimensional reflectance can be identified with the reflectance of three-dimensional medium at a small phase angle. Our laboratory spectral and photometric measurements of powdered color glasses (e.g., Shkuratov 1987) have shown that, in the limits of 10%, the measured albedo at the phase angle of about 5^0 can be identified with albedo (reflectance) A derived from the one-dimensional model. This albedo can be used to estimate the brightness coefficient at arbitrary phase angles α: $B = A \cdot f(\alpha)$, where $f(\alpha)$ is the phase function normalized at 5^0.

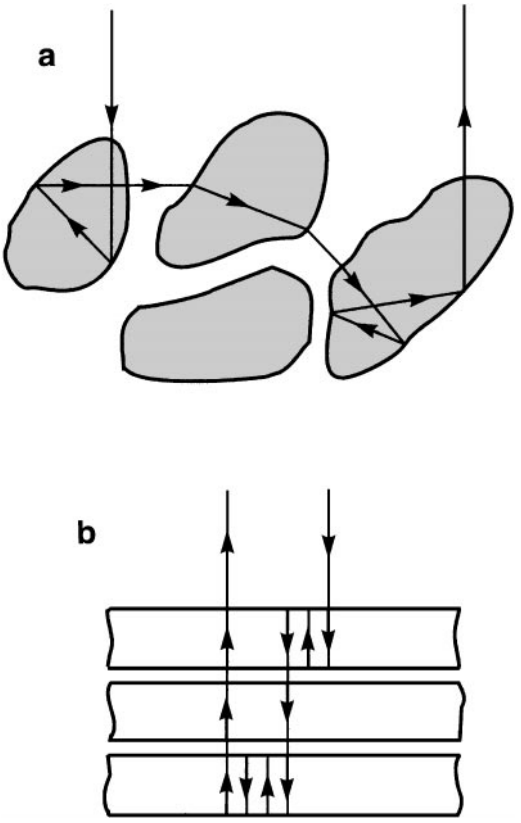

FIG. 1. A scheme of light propagation: (a) through a particulate medium and (b) through plates in a pile.

FORMULATION OF THE BASIC MODEL

Consider a powdered surface (a medium) composed of semitransparent particles of arbitrary form and of sizes much greater than the wavelength λ. Let a parallel light beam be incident on the boundary of the medium. Ray propagation in such medium is a random branching process. The branching points are characterized by two values, namely, the reflection $R(n^*, \theta)$ and transmission $T(n^*, \theta)$ coefficients, where n^* is the complex refractive index of the material ($n^* = n - i\kappa$, where n and κ are the optical constants—the real and imaginary parts of the refractive index, respectively) and θ is the local angle of incidence on the particle interface. The intervals between the branching points are characterized by optical density $\tau = 4\pi\kappa S/\lambda$, where S is the effective (average) optical pathlength, κ and τ being equal to zero in the interstitials. In terms of the variables, the extinction I/I_0 can be determined for any trajectory of a ray in the medium

(I_o and I are intensities of light in the points of entrance and exit, respectively). Summation over all ray trajectories, i.e., over all entrance points and all branching points for each entrance point provides the intensity of light reflected by the medium.

Method of summation. For an analytic summation, different methods are applied. To demonstrate one of them, we use a simple example. Consider a ray incident on the particle interface at an angle θ_{in}. Refracting into the particle the ray is reflected m times from the internal side of the particle interface at angles θ_ν ($\nu = 1 - m$) and then emerges from the particle at an angle θ_{em}. The intensity of the ray is

$$I = I_o \cdot T(\theta_{em}) \cdot T(\theta_{in}) \cdot \exp\left(-\frac{4\pi\kappa}{\lambda}\sum_{\nu=0}^{m} s_\nu\right) \cdot \prod_{\nu=0}^{m} R(\theta_\nu), \quad (1)$$

where $T(\theta_{in})$ and $T(\theta_{em})$ are the transmission coefficients for light coming and outgoing, $R(\theta_\nu)$ is the reflectance coefficient for νth reflection by the internal side of particle interface (at $\nu = 0$, $R = 1$), and s_ν is the distance between internal reflections. Now a subset of rays scattered by the particle such that the rays in the subset are distinguished by the entrance angles θ_{in} can be considered. Summing (averaging) all the rays yields

$$\bar{I} = I_o \cdot \bar{T}_{in} \cdot T(\theta_{em}) \cdot \prod_{\nu=0}^{m} R(\theta_\nu) \cdot \exp\left(-\frac{4\pi\kappa}{\lambda}\sum_{\nu=0}^{m} s_\nu\right). \quad (2)$$

We can repeat this procedure for the angle θ_{em}, each angle θ_ν, and distance s_ν. Then

$$\langle I\rangle = I_o \cdot \bar{T}_{in} \cdot \bar{T}_{em} \cdot \prod_{\nu=0}^{m} \bar{R}(\theta_\nu) \cdot \overline{\exp\left(-\frac{4\pi\kappa}{\lambda}\sum_{\nu=0}^{m} s_\nu\right)}. \quad (3)$$

The average path length S in the particle between two internal reflections is defined as

$$\overline{\exp\left(-\frac{4\pi\kappa}{\lambda}\sum_{\nu=0}^{m} s_\nu\right)} = \exp\left(-\frac{4\pi\kappa}{\lambda} mS\right). \quad (4)$$

Below we ignore the symbols of averaging and use the following designation: T_e and T_i are the average transmittances for light penetrating into particle from outside and in the opposite direction, respectively, and R_i is the average coefficient of internal reflection inside particle.

Albedo of a particle. Denote r_b and r_f the fractions of light flux scattered by a particle into the backward and forward hemisphere, respectively. They can be presented as series on multiplicity scattering, where the first term is the fraction of the incident flux reflected by the surface of a particle, the second one describes the flux transmitted through a particle, the third one takes an internal reflection into account, and so on; i.e.,

$$\begin{aligned} r_b &= R_b + W_2 T_e T_i \exp(-\tau) + W_3 T_e T_i R_i \exp(-2\tau) + \cdots \\ &= R_b + T_e T_i \sum_{m=1}^{\infty} W_{m+1} R_i^{m-1} \exp(-m\tau), \end{aligned} \quad (5a)$$

$$\begin{aligned} r_f &= R_f + (1 - W_2) T_e T_i \exp(-\tau) \\ &\quad + (1 - W_3) T_e T_i R_i \exp(-2\tau) + \cdots \\ &= R_f + T_e T_i \sum_{m=1}^{\infty} (1 - W_{m+1}) R_i^{m-1} \exp(-m\tau), \end{aligned} \quad (5b)$$

where τ is defined in the beginning of this section, W_m are the probabilities for the beam to emerge backward at mth scattering, R_b and R_f are the average (backward and forward) reflectance coefficients. They are

$$\begin{aligned} R_b &= \frac{\int_0^{2\pi} d\psi \int_0^{\pi/4} d\theta \cdot R_o(n,\theta) \cdot \cos\theta \cdot \sin\theta}{\int_0^{2\pi} d\psi \int_0^{\pi/2} d\theta \cdot \cos\theta \cdot \sin\theta} \\ &= 2\int_0^{\pi/4} d\theta \cdot R_o(n,\theta) \cdot \cos\theta \cdot \sin\theta, \end{aligned} \quad (6a)$$

$$\begin{aligned} R_f &= \frac{\int_0^{2\pi} d\psi \int_{\pi/4}^{\pi/2} d\theta \cdot R_o(n,\theta) \cdot \cos\theta \cdot \sin\theta}{\int_0^{2\pi} d\psi \int_0^{\pi/2} d\theta \cdot \cos\theta \cdot \sin\theta} \\ &= 2\int_{\pi/4}^{\pi/2} d\theta \cdot R_o(n,\theta) \cdot \cos\theta \cdot \sin\theta, \end{aligned} \quad (6b)$$

where R_o is the Fresnel coefficient. The value R_i can be found as

$$\begin{aligned} R_i &- \frac{\int_0^{2\pi} d\psi \int_0^{\pi/2} d\theta \cdot R_o\left(\frac{1}{n},\theta\right) \cdot \cos\theta \cdot \sin\theta}{\int_0^{2\pi} d\psi \int_0^{\pi/2} d\theta \cdot \cos\theta \cdot \sin\theta} \\ &= \frac{n^2 - 1}{n^2} + 2\int_0^{\theta_o} d\theta \cdot R_o\left(\frac{1}{n},\theta\right) \cdot \cos\theta \cdot \sin\theta, \end{aligned} \quad (6c)$$

where $\theta_o = \arcsin(1/n)$ is the angle of the full internal reflection. The average transmittances T_e and T_i are calculated in the same way by averaging transmission coefficients.

For a homogeneous particle (without a thin light-absorbing layer on the surface) there are simple relations between the values of R- and T-type. Denote $R_e = R_b + R_f$. Then

$$T_e = 1 - R_e, \qquad T_i = 1 - R_i. \quad (7a)$$

Integration of (6c) gives

$$T_i = T_e/n^2, \qquad R_i = 1 - (1 - R_e)/n^2. \quad (7b)$$

Calculations of R_b, R_e, and R_i in the range of $n = 1.4$–1.7 showed the following empirical approximations to be satisfactory:

$$R_b \approx (0.28 \cdot n - 0.20) R_e, \tag{8a}$$

$$R_e \approx r_o + 0.05, \tag{8b}$$

$$R_i \approx 1.04 - 1/n^2, \tag{8c}$$

where $r_o = (n-1)^2/(n+1)^2$ is the Fresnel coefficient at the normal incidence. Due to the total internal reflection, R_i is always larger than R_e. Note that the approximation (8b) has been published by Hapke (1981).

Now we evaluate the probabilities W_m. This is easy to do for a large order of scattering when a light beam "forgets" its initial direction and all directions become equally probable—for this case $W_m = 1/2$. Such an estimation is not correct for small m because $W_2 = 0$, since the light transmitted through a particle without internal reflections cannot be directed toward the source. Unfortunately, in the frames of the approach proposed, a more detailed estimation of W_m is impossible; so we assume further that $W_2 = 0$ and $W_m = 1/2$ for $m > 2$. In this assumption, the series become geometric progressions and are easily summated:

$$r_b = R_b + \frac{1}{2} T_e T_i R_i \exp(-2\tau)/(1 - R_i \exp(-\tau)), \tag{9a}$$

$$r_f = R_f + T_e T_i \exp(-\tau) + \frac{1}{2} T_e T_i R_i \exp(-2\tau)/ (1 - R_i \exp(-\tau)). \tag{9b}$$

Thus, the values r_b and r_f represent the one-dimensional (angularly averaged) light scattering indicatrix of a particle. It is interesting to calculate the parameter of indicatrix asymmetry: $\eta = r_f/r_b$. In Fig. 2 the value η is given as a function of absorption. As one can see, the ratio r_f/r_b versus τ has a maximum at τ near 0.2.

Albedo of a particulate surface. The next problem is to use the indicatrix of a particle to calculate the albedo (reflectance) A of a surface. Denote q the volume fraction filled by particles. For a randomly packed medium, there is a mathematical theorem that the area fraction filled by particles in an intersecting plane (or a line) is equal to q. Thus, the one-dimensional indicatrix for a layer is

$$\begin{aligned} \rho_b &= q \cdot r_b \\ \rho_f &= q \cdot r_f + 1 - q. \end{aligned} \tag{10}$$

The albedo of a half-infinite pile of the layers can be calculated as series on order of scattering between the layers

$$A = \rho_b + \rho_f^2 A + \rho_f^2 \rho_b A^2 + \cdots = \rho_b + \rho_f^2 A/(1 - \rho_b A). \tag{11}$$

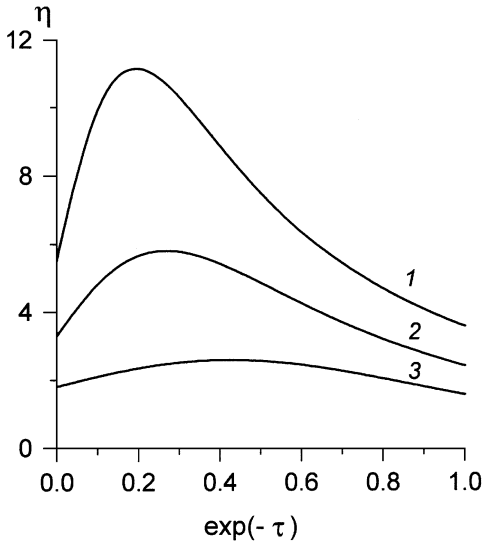

FIG. 2. The asymmetry $\eta = r_f/r_b$ of the one-dimensional indicatrix of a particle as a function of its optical density at different values of refractive index. Curves 1, 2, and 3 correspond to the following n: 1.33, 1.55, and 2.0.

Then

$$A = \frac{1 + \rho_b^2 - \rho_f^2}{2\rho_b} - \sqrt{\left(\frac{1 + \rho_b^2 - \rho_f^2}{2\rho_b}\right)^2 - 1}. \tag{12}$$

Inversion of the model. An important characteristic of the model is its invertibility, i.e., the imaginary part κ of the surface material can be found, if the albedo is known and estimations for the parameters n, S, and q are available. The relations (12) can be considered as equations for κ and exactly solved,

$$\kappa = -\frac{\lambda}{4\pi S} \ln\left[\frac{b}{a} + \sqrt{\left(\frac{b}{a}\right)^2 - \frac{c}{a}}\right], \tag{13}$$

where

$$\begin{aligned} a &= T_e T_i (y R_i + q T_e), \\ b &= y R_b R_i + \frac{q}{2} T_e^2 (1 + T_i) - T_e (1 - q R_b), \\ c &= 2y R_b - 2T_e (1 - q R_b) + q T_e^2, \\ y &= (1 - A)^2/2A. \end{aligned}$$

Note once again two advantages of our model: (1) as distinct from others, our model includes explicit dependence on porosity and enables us to calculate its effect; (2) the model is analytically invertible, i.e., explicit formulae are derived that allow calculations of the imaginary part of refractive index from albedo value, if *a priori* data on the real part of refractive index and surface porosity are known.

Relative importance of each parameter. Our model contains four parameters: n, κ, S, and q. Consider their effect on the function $A(n, \kappa, S, q)$.

In Figs. 3a and 3b results of calculations of the dependence of A on n and q are presented. The variations of n and q are of minor influence at high albedos (small τ) and rather significant at low ones. That porosity does not affect much the albedo of bright particulate surfaces is well known from the experiments of Adams and Filice (1967). Curves in Figs. 3a and 3b show that changing the optical density τ of the particles (i.e., the product κS) affects albedo most strongly. This fact together with the possibility of *a priori* estimation of the values n, q, and S enable us to solve the problem of calculation of $\kappa(\lambda)$ for surfaces of atmosphereless celestial bodies using the measured spectra $A(\lambda)$.

Experimental. To test the model experimentally, two $\kappa(\lambda)$ functions for a semitransparent homogeneous material are compared: (1) a function calculated from transmission spectrum of a solid slab and (2) a function calculated from the albedo spectrum of a powdered material using the model. This approach was already used by Hapke and Wells (1981) and Shkuratov (1987).

We measured three types of filter glasses. Transmission of the filters was found in the range 0.3–0.9 μm (Fig. 4a) by the spectrometer EPS-3T. Then the filters were ground. A grain-size fraction between 40 and 60 μm was obtained by sieving, so we can estimate the value of S as 50 μm. The reflectance spectra of the powders were measured with the same spectrophotometer (Fig. 4b). This instrument allowed determinations of $A(\lambda)$ at the phase angle 5°. More details of these experiments are presented in Shkuratov (1987). The functions $\kappa(\lambda)$ were calculated using transmission and reflectance spectra. Formula (13) was applied with $n = 1.53$ known for the optical filters used. In spite of the rough data on the particle size and n, Fig. 4c shows rather good agreement of the results.

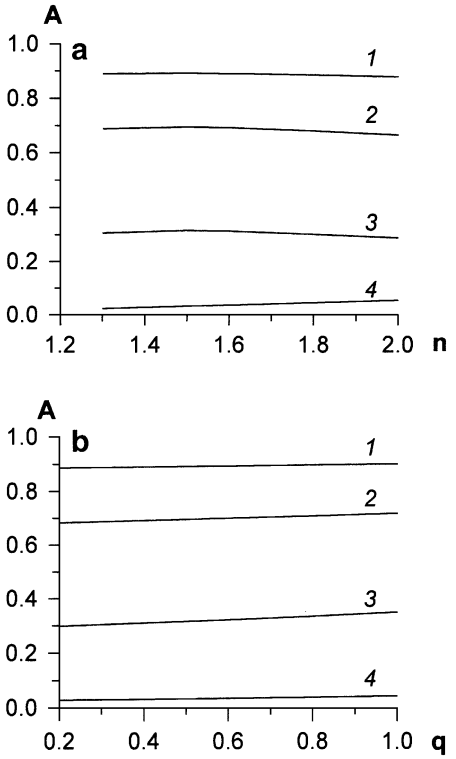

FIG. 3. Albedo vs refractive index n (a) and on volume concentration q of particles (b). Curves 1, 2, 3, and 4 correspond to the following τ: 0.001, 0.01, 0.1, and 1.

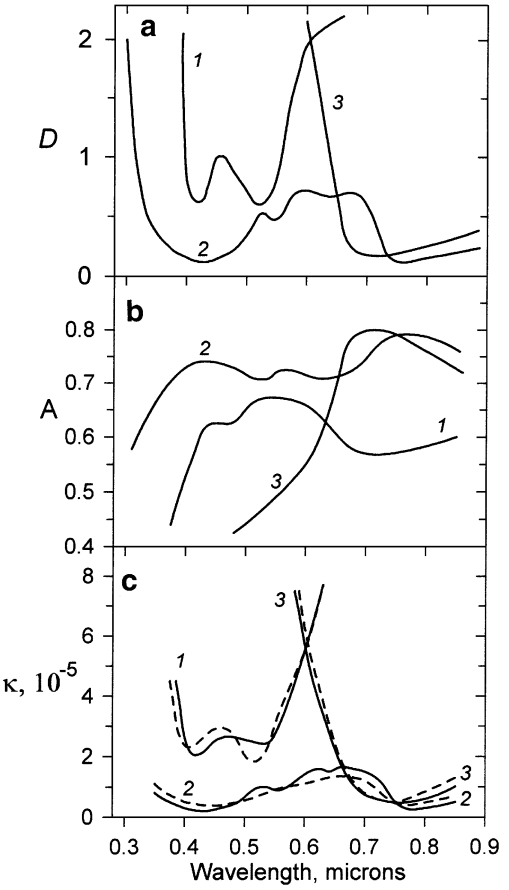

FIG. 4. Spectra of green, blue, and red filter glasses: curves 1, 2, and 3, respectively. Plot (a) corresponds to transmission spectra of the glasses, (b) reflectance spectra of the powdered samples, and (c) calculated spectra $\kappa(\lambda)$ derived from the transmission ones by usual procedure (solid lines) and from the reflectance spectra with our model (dashed lines).

GENERALIZATION TO MULTICOMPONENT SURFACES

The surfaces of atmosphereless celestial bodies have complex composition and structure. They are multicomponent and multiscale. Nevertheless, in light-scattering problems, such surfaces are usually considered as media with average optical constants. This approach is evidently restricted. The advantage of our model is its simple generalization to the multicomponent case.

Models of the surfaces. The solar wind and meteoritic bombardment of atmosphereless celestial bodies affect the composition and structure of their surfaces changing their optical properties. These effects take place in all scales of surface structure—from angstroms to tens of micrometers (solar wind and the processes of impact sputtering evaporation and condensation) and from micrometers to hundreds of kilometers (mixing of the surface material by meteoritic impacts).

For optical properties the relation of the scale of inhomogeneity to wavelength λ is important. When the size $S \gg \lambda$, methods of geometrical optics are used; if $S \leq \lambda$, we have to deal with diffraction problems. We consider four types of surface structure.

(1) Mixture of coarse (of size $\gg\lambda$) particles. They can be dark or transparent with different contribution of multiple scattering.

(2) Coarse transparent particles contain fine (of size $\ll\lambda$) inclusions of an absorbing component. Such inclusions do not affect the refraction (n) of the particles but increase absorption (κ), if their optical density is ≥ 1.

(3) Coarse particles are surrounded by thin (of thickness $\leq\lambda$) absorbing films. Such films change both refraction and absorption of the particle surfaces.

(4) Coarse transparent particles are heterogeneous in scale $\ll\lambda$. Such particles can be considered as quasihomogeneous with effective optical constants which should be calculated. Then the medium can be considered as in point (1).

Practically all real structures can be presented as a combination of the structures mentioned above. Light scattering by each of them can be described by some generalization of the basic model.

Mixture of coarse particles. In this case, the generalization of the basic model is trivial because the model is, in fact, two-component: the surface contains solid particles and pores of a size $\gg\lambda$. If c_j is the concentration of the jth solid component, the one-dimensional indicatrix for a layer is similar to (10)

$$\begin{aligned} \rho_{\mathrm{b}} &= q \sum_j (c_j r_{\mathrm{b},j}) \\ \rho_{\mathrm{f}} &= q \sum_j (c_j r_{\mathrm{f},j}) + 1 - q. \end{aligned} \tag{14}$$

Substituting (14) in (12) we obtain the albedo for a mixture of coarse particles.

Coarse particles with fine absorbing independent inclusions. The components with particle size $\ll\lambda$ are inclusions in the bulk or near the surfaces of coarse particles. For such a small size, surface tension of the inclusions is very strong and, therefore, the shape of particles is close to spherical. To find the contribution of the inclusions to light scattering, the Mie theory may be applied. According to this theory the contribution of absorbing inclusions to the imaginary part of refractive index can be presented as

$$\kappa_{\mathrm{a}} = \frac{3}{2} c \cdot n \cdot \mathrm{Im} \frac{\varepsilon - 1}{\varepsilon + 2}, \tag{15}$$

where c is the volume concentration of the inclusions, n is the real part of the matrix refractive index, and ε is the ratio of the complex dielectric constant of the inclusions to that of matrix. To find the albedo by formula (12), the sum $\kappa + \kappa_{\mathrm{a}}$ is used instead of κ.

Because of the effect of environment, fine inclusions of absorbing matter frequently occur near the surface of the particles in a layer of a thickness $d \ll \lambda$. In particular, fine inclusions of the reduced iron are formed in lunar regolith due to the reducing effect of solar wind and heating in the impact processes. If such inclusions are present, the optical density of the particles increases because a light beam passes the absorbing layer twice per each scattering. It gives

$$\kappa_{\mathrm{eff}} = \kappa + \frac{2d}{S} \kappa_{\mathrm{a}}. \tag{16}$$

The Mie theory can be applied only for small concentration of the inclusions ($c \ll 1$). For large values of c the methods described below should be used.

Coarse particles covered by thin absorbing films. If the thin (of thickness $d \ll \lambda$) absorbing layer is a coating on the particles, both absorption and refraction at the particle surfaces are changed (Starukhina and Shkuratov, 1996). In this case, instead of the Fresnel coefficients the following values should be integrated in formulas (6a)–(6c),

$$R_{13} = \left(|r_{13}^{\parallel}|^2 + |r_{13}^{\perp}|^2\right)/2, \qquad T_{13} = \left(|t_{13}^{\parallel}|^2 + |t_{13}^{\perp}|^2\right)/2, \tag{17a}$$

where

$$r_{13} = \frac{r_{12} + r_{23}\Phi}{1 + r_{12} r_{12} \Phi}, \qquad t_{13} = \frac{t_{12} t_{23} \sqrt{\Phi}}{1 + r_{12} r_{12} \Phi}, \tag{17b}$$

and $\Phi = \exp(4\pi i n_{\mathrm{f}}^* d \cos\theta/\lambda)$, n_{f}^* being the complex refractive index of the coating material. For simplicity, we omit the polarization signs $\parallel$ and $\perp$ in (17b). Indices 12 and 23 in r and t (Fresnel coefficients of reflection and transition) correspond to the boundaries vacuum–film and film–substrate, respectively.

Microheterogeneous particles. If particles are heterogeneous in the scale $\ll\lambda$, neither of the components can be interpreted as "matrix" and the particles can be considered as homogeneous with an effective dielectric constant ε. To calculate ε for a random microheterogeneous mixture of components with concentrations c_j and dielectric constants e_j, the Bruggeman relation can be used (Bohren and Huffman 1983),

$$\sum_j c_j \frac{\varepsilon_j - \varepsilon}{\varepsilon_j + 2\varepsilon} = 0. \tag{18}$$

Finally, note again that as distinct from, e.g., the Kubelka-Munk formula which deals with two effective parameters of a medium, the suggested model uses spectra of optical constants of the medium materials. In our model all stages of the spectroanalytic experiment according to Rosenberg's scheme are realized in a simplified form. As a result, $\kappa(\lambda)$ can be estimated using data on $A(\lambda)$ if the values of n and q are known.

IMPLICATIONS TO OPTICS OF THE MOON

In this section we consider implications of the presented model and its generalizations for spectrophotometry and colorimetry of the Moon.

Estimation of the average $n(\lambda) - i\kappa(\lambda)$. Studies of the optical properties of lunar soils and surfaces of other planetary bodies require estimations of the average values of the optical constants. In many laboratory studies (petrological, mineralogical, chemical), the values of n and κ are not usually determined. There is a lack of n and κ data for the lunar soils over a wide spectral range. Such data were published for three terrestrial samples (basalt, basaltic glass, and obsidian) by Pollack *et al.* (1973) and Lamy (1978). The first two types of samples can be considered as some analogs of lunar material. On the base of our model we estimated the optical constants of an "average Moon."

In Fig. 5a, we present a composite albedo spectrum of the Moon using lunar observation data as well as laboratory measurements of lunar samples (Carver *et al.* 1975, Henry *et al.* 1976, Wu and Broadfoot 1977, Dementyev and Markov 1978, Pieters 1978, Pieters *et al.* 1993). In the UV range, a broad band caused by transitions between valence and conduction bands occurs. Also in this range, strong oxygen-to-metal charge transfer bands take place. The longwave wing of this UV absorption ranges up to 4 μm. On its background only comparatively weak absorption features at 1 and 2 μm are observed. The features are due to d–d electron transitions in Fe^{2+} ions in minerals of olivine and pyroxene types. The spectral fall-off at $4 < \lambda < 8$ μm is due to ion vibrations.

In order to calculate the spectrum $\kappa(\lambda)$, the function $n(\lambda)$ is required. The result of the calculation of κ being not very sensitive to the value of n, we take the "basaltic" $n(\lambda)$ (Pollack *et al.* 1973, Lamy 1978) as the lunar one (see Fig. 5b). In Fig. 5c $\kappa(\lambda)$ calculated on the base of our model and extended by UV data from (Pollack *et al.* 1973, Lamy 1978) is shown, the effective optical pathlength S being taken as 60 μm.

Effect of particle size on absorption band depth. Among the parameters of reflectance spectra, only albedo is usually considered to be dependent on particle size. To eliminate the dependence, spectral curves are normalized.

The other spectral parameters, namely, relative depth of bands H (see Fig. 6) and spectral slopes (color-indices), are often used to compare the normalized spectra and to characterize the abundance of absorbing materials. However, spectral studies demonstrate that powders of the same materials but with different particle sizes show pronounced distinctions in the spectral

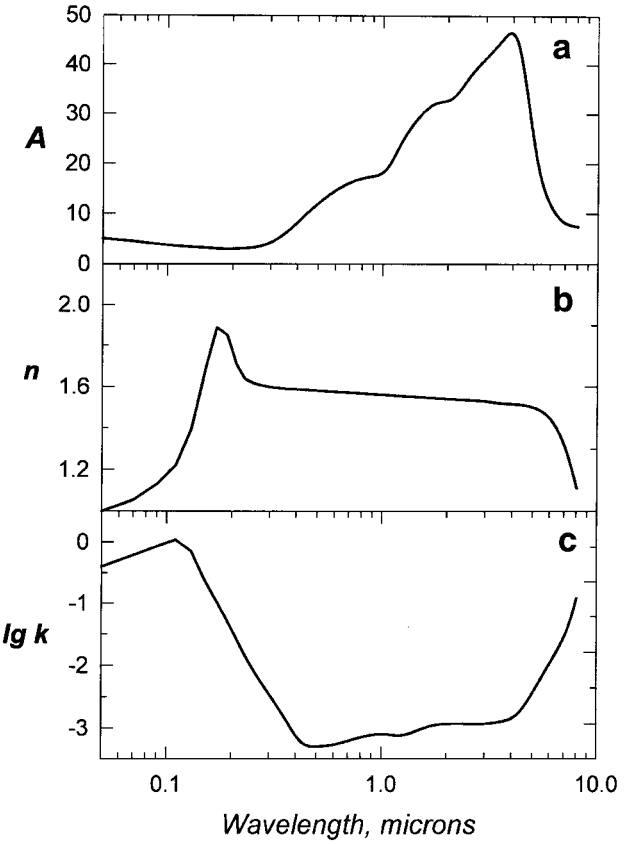

FIG. 5. Composite spectra of albedo (a), and real (b), and the imaginary (c) parts of the refractive index for the "average Moon."

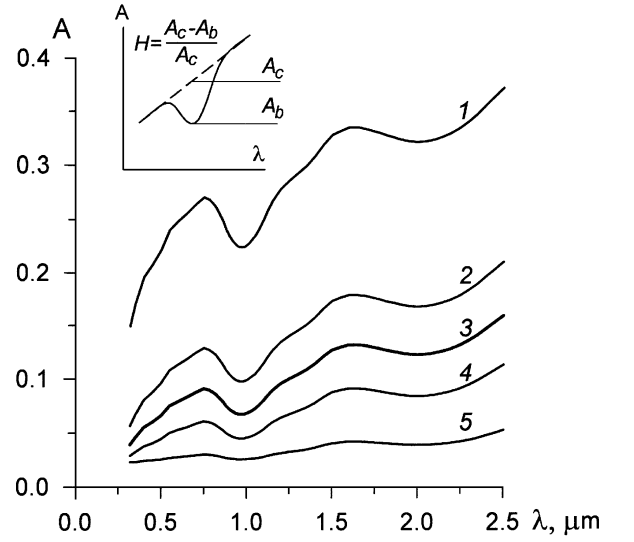

FIG. 6. The model spectra of the lunar sample 24085 for particle sizes 20 μm (line 1), 50 μm (line 2), 100 μm (line 4), and 200 μm (line 5) calculated starting with the spectrum of the fraction 45–94 μm (line 3, the mean particle size 70 μm and $q = 0.7$ was taken); the insertion shows the used definition of the relative band depth.

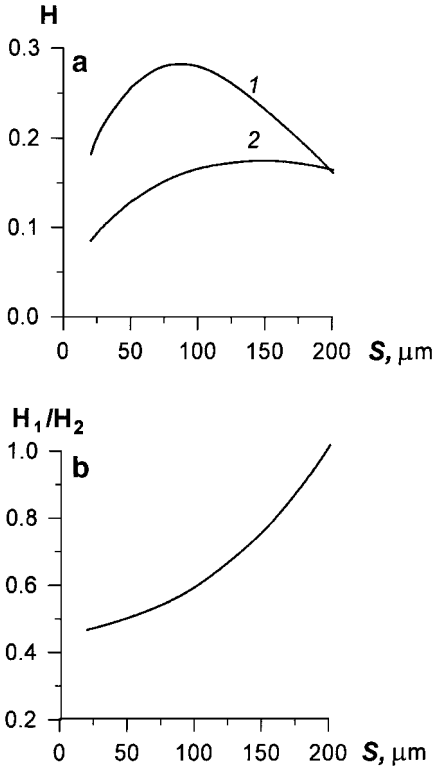

FIG. 7. Particle size dependence (a) for the depths of the absorption bands at 0.95 μm (line 1) and at 2.0 μm (line 2) calculated from the fraction 45–94 μm of the lunar sample 24085; (b) for the ratio of 2.0- to 0.95-μm band depths. The spectra used are provided in Fig. 6.

contrast of bands even in normalized spectra (e.g., Adams and Filice 1967, Shkuratov 1987). Powders with large particles are so dark that bands are almost indistinguishable. On the other hand, powdering of low-absorbing materials into small particle size separates can also attenuate the bands.

The theoretical model described above was used to calculate the particle size dependence of parameters of normalized spectra of lunar soils. Starting from the albedo spectrum of a lunar sample with known particle size, the spectrum of the imaginary part of the refractive index was found. Then the albedo spectra with different particle sizes were calculated. For calculations we have taken the spectrum of the fraction 45–94 μm of the sample 24085 of Luna 24 (Pieters *et al.* 1993). An example of such calculations is shown in Fig. 6. Using the spectrum of the fraction 45–94 μm (the average particle size of 70 μm was taken), spectra for particle sizes 20, 50, 100, and 200 μm were calculated assuming the same composition for all fractions.

From these data we determined the particle size dependences of the depths of the absorption bands at 0.95 and 2.0 μm. The results are presented in Fig. 7a and show that the spectral contrast is minimal for small and for large particles. The ratio between the band depths also turned out to be particle size dependent, as it can be seen in Fig. 7b for the ratio of band depths at 2.0 and 0.95 μm. The latter seems to contradict experimental measurements by Cloutis *et al.* (1986) who claim the band ratio to be invariant with particle size. However, this can be easily explained: for the majority of the Cloutis *et al.* (1986) spectra, the 0.95- and 2.0-μm bands are situated almost on the same albedo level and, therefore, they are transformed by model calculations equally.

The particle size dependences of color indices C(0.65/0.40 μm), C(2.50/0.75 μm), and C(0.95/0.75 μm) are given in Fig. 8 for the mare (Luna-16) and highland (Luna-20) samples. The shape of the curves is the same as for the band depths, with a maximum of spectral contrast in the size range 40–100 μm. Note that particle size dependence of C(0.95/0.75 μm) is not pronounced because this color index is close to 1.

Natural surfaces consist of different size fractions. However, for each surface a characteristic size, which dominates its optical properties in the spectral range considered, exists. This size can vary for different surfaces. So, particle size dependence of band depths and spectral slopes should be taken into account in interpretation of telescope as well as laboratory spectral measurements.

Simulation of the albedo-color diagram. Studies of albedo-color diagrams enable to predict the chemical composition of the lunar surface (e.g., Lucey *et al.* 1995). Using our model we can

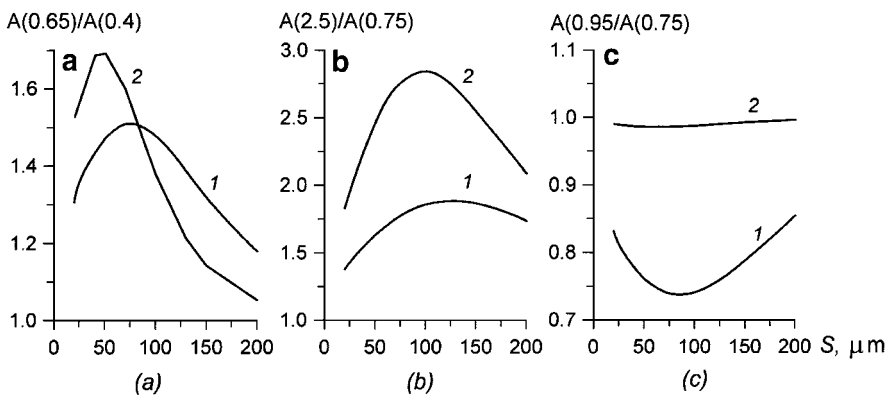

FIG. 8. Particle size dependences of color indices in the visible and infrared ranges: (a) C(0.65/0.40 μm), (b) C(2.50/0.75 μm), and (c) C(0.95/0.75 μm). Curves 1 and 2 correspond to the mare and highland samples. The spectra used are provided in Fig. 10.

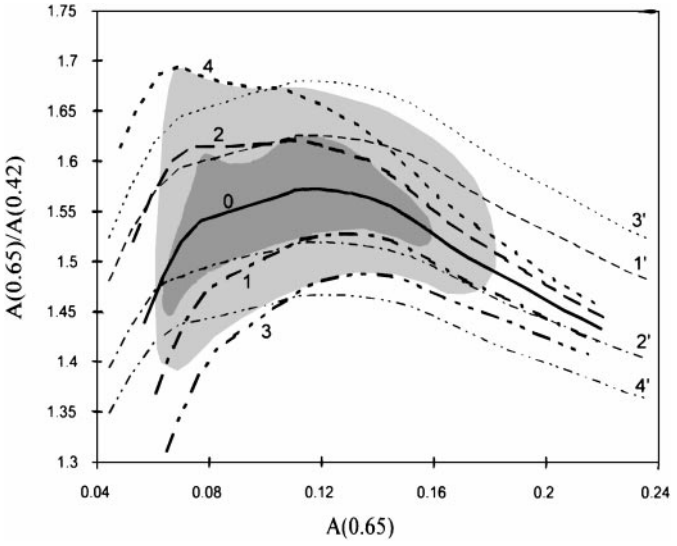

FIG. 9. A lunar albedo (0.65 μm)–color (0.65/0.42 μm) diagram. The shadowed area corresponds to the observation data for the nearside of the Moon (Shkuratov *et al.* 1997). The model diagram (curves) is calculated as follows. The values of $\kappa(0.65\ \mu\text{m})$ were varied within the limits 10^{-4}–10^{-3} to cover the albedo range of the Moon. The different curves were obtained by variations of n, q, and $\kappa(0.42\ \mu\text{m})$. The basic combination of parameter values (curve 0) is $n=1.6$, $q=0.7$, $S=50\ \mu$m, the average values of $\kappa(0.42\ \mu\text{m})$ for each point of the basic curve being found from lunar data (see text). Bold lines are the albedo-color curves for the average values of $\kappa(0.42\ \mu\text{m})$, $q=0.7$, and $n=1.7$, 1.5 (lines 1, 2), 1.8, and 1.4 (lines 3 and 4), respectively. Thin lines are those for $n=1.6$, $q=0.7$, and $\kappa(0.42\ \mu\text{m})$ changed near the average values +3% (line 1′), −3% (line 2′), and +6% (line 3′) and −6% (line 4′), respectively.

simulate the diagrams. It allows us to find out which of the physical parameters of the surface material control the diagram shape.

Figure 9 shows a scheme of the diagram $A(0.65\ \mu\text{m})$–$C(0.65/0.42\ \mu\text{m})$ developed by Shkuratov *et al.* (1997) for the near side of the Moon. For each value of $A(0.65\ \mu\text{m})$, the average value of color index was determined (curve 0), and the corresponding values of κ for both wavelengths were calculated with $n=1.60$, $q=0.7$, and $S=50\ \mu$m. Using the parameters of the average curve we simulated the albedo-color diagram. The values of $\kappa(0.65\ \mu\text{m})$ were varied within the limits 10^{-4}–10^{-3} to cover the albedo range. The color-index variations have been obtained in two ways: (1) by variation of n and q using the average values of $\kappa(0.42\ \mu\text{m})$, (2) by variation of $\kappa(0.42\ \mu\text{m})$.

Bold lines in Fig. 9 are the albedo-color curves for the average values of $\kappa(0.42\ \mu\text{m})$ and $q=0.7$ for $n=1.4$, 1.5, 1.6, 1.7, and 1.8. Thin lines correspond to $q=0.7$, $n=1.6$, and $\kappa(0.42\ \mu\text{m})$ changed in the range ±3 and $\pm6\%$. Our simulation has shown that: (1) the widths of diagrams cannot be explained by variation of porosity of the surface material; (2) the width of the high albedo part of the diagram ($A>0.1$) is not due to variations of n but can be explained by variations of $\kappa(0.42\ \mu\text{m})$ in the range of only $\pm3\%$; (3) the diagram shapes at low albedo parts ($A<0.1$) are not reproduced by $\kappa(0.42\ \mu\text{m})$ variations. The best fit is achieved by variations of n in the range of ±0.2 from the average value.

Effect of reduced iron on spectra of lunar soils. The optical properties of lunar soils are mainly determined by the fine fraction. This is confirmed, in particular, by data presented in Fig. 10 (Pieters *et al.* 1993). Here, one can compare the spectral curves for the original samples of the mare (Luna 16) and highland (Luna 20) lunar soils and for their particle size separates: data for the original sample and for the fine separate (<45 μm) are rather close.

Owing to the high surface/volume ratio, small particles of the lunar regolith are expected to be most sensitive to the processes resulting from exposure to space environment. Among such processes, the formation of superfine (<300 Å) inclusions of the reduced iron both near the surface (Hapke *et al.* 1975, Gold *et al.* 1975, Dikov *et al.* 1978) and in the bulk (Morris 1977) of lunar particles is known to take place. The question arises: is the distinction of the spectra of the original samples and fine separates due to particle size only or to the processes on the surface as well (Pieters *et al.* 1993; Starukhina *et al.* 1994)?

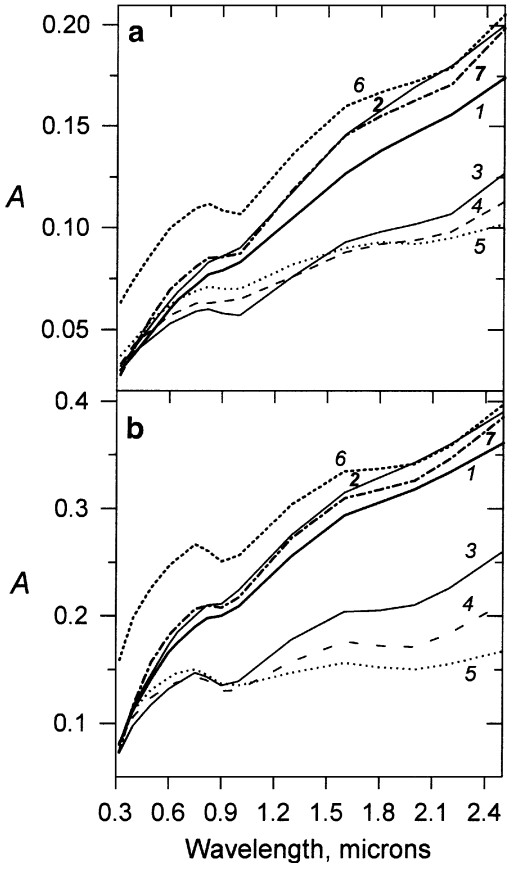

FIG. 10. Reflectance spectra of particle size separates of lunar soils. (a) Mare (1637, Luna 16), (b) highland (2014, Luna 20); 1, original samples; 2, fraction <45 μm, 3, fraction 45–94 μm; 4, fraction 94–250 μm; 5, fraction 250–1000 μm; 6, calculated spectra for samples of the same composition as 45- to 94-μm fractions (curves 3) but for particle size 40 μm; 7, the same as 6 but for particles with volume concentration of superfine reduced iron 2×10^{-4} for mare soil and 10^{-4} for highland one.

For particles of complicated structure (aggregates), the value of S is less than the average size of the particles and equals approximately the average size of grains composing the particles, but this size is not known. We supposed that most of the particles of the fine (<45 μm) fractions consist of one grain and assumed that, in this case, the size S is approximately 40 μm. To estimate S for coarse fractions, we supposed that the values of κ for the fine fractions are at least not smaller than those for the coarser ones in the whole spectral range. This assumption is supported by the consideration that small particles should be most sensitive to the processes resulting from surface exposure which are known to darken lunar soils. In this assumption, the size of S for the 45–94 μm fractions turned out to be about twice as large as that for <45-μm ones. We used $S = 80$ μm.

We calculated the spectra of the 45- to 94-μm fractions as they would be, if their particles were as small as those of <45-μm fractions. As shown in Fig. 10 (curves 6), if the particles of the <45-μm fractions were chemically identical to those of the 45- to 94-μm ones, the <45-μm fractions would be: (1) much brighter in the visible range, (2) with more pronounced 1 μm feature, and (3) with less red spectral slope (Starukhina *et al.* 1994).

We supposed that the difference is due to the submicrometer inclusions of reduced iron in lunar particles. If the Fe^0 inclusions are located near the surfaces of the regolith particles, their effect can be taken into account by substituting the value $\kappa_{\rm eff}$ from formula (16) instead of κ. According to (16), the contribution of the colloid iron increases with decreasing grain size. Therefore, the spectra of the smallest fractions are expected to be mostly affected by the presence of reduced iron. We calculated the spectra of the material of the 45- to 94-μm fraction with particles of 40 μm size surrounded by a layer $d = 1000$ Å of colloid iron, taking the optical constants of iron by Johnson and Cristy (1974). Calculated spectra (curves 7 in Fig. 10) turned out to be close to the spectra of the <45-μm fractions at Fe^0 concentration $c = 4\%$ for the mare and 2% for the highland.

The values of thickness d and the ratio between the concentrations for mare and highland soils are about the observed ones (Gold *et al.* 1975, Dikov *et al.* 1978), but the concentrations are an order of magnitude higher as observed. The explanation is that mature particles contain most of the superfine reduced iron in the bulk and not near the surface (Morris 1977). If the spectral differences between the fractions are due to the bulk Fe^0, the addition to κ in formula (15) should be used. To obtain the same model spectra for the fractions <45 μm, as shown in Fig. 10 (lines 7), a bulk volume concentration of about 0.01% has to be used. This seems to be reasonable because it is about 10 times less than the greatest volume concentrations of total Fe^0 in the lunar regolith (Morris 1977).

Effect of reduced iron on the position of d–d bands in pyroxene and olivine. The pyroxene adsorption bands near 1 and 2 μm and the olivine 1-μm band are known to be shifted longward with increasing Fe^{2+} content. This has been proposed to be used for remote sensing data analysis (Adams 1974). However, using this method for the surfaces of atmosphereless celestial bodies, the effect of cosmogenic factors (e.g., iron reduction) should be taken into account. As has been shown above, the presence of reduced iron increases the spectral slope and decreases the band depth. Evidently, the increase of the red spectral slope should shift the spectral position of the minimum of absorption bands to shorter wavelengths, i.e., to the opposite direction as compared to the shift due to the presence of Fe^{2+}. In order to study this effect we applied our model to convert reflectance spectra of orthopyroxene and olivine powders into the spectra of κ. We used reflectance spectra measured by Pieters (1988, pers. commun.). The obtained κ spectra were modified using formula (15) in order to take superfine reduced iron into account. Then new reflectance spectra for such materials were calculated. With the increase of reduced iron concentration, the red slope of the spectra increases and the position of the bands near 1 and 2 μm shifts shortward as shown in Fig. 11 for olivine and in Figs. 12a and 12b for orthopyroxene. The blue shift of the 1-μm bands per each vol% of Fe^0 is about 0.5 and 0.1 μm for olivine and orthopyroxene, respectively. The blue shift of the 2-μm band of orthopyroxene is about 0.2 μm per each vol% of Fe^0. The shifts can be compared to the red shifts due to the increase of Fe^{2+} content (about 0.004 μm per 10% of the ratio $Fe^{2+}/(Fe^{2+} + Mg^{2+})$ for the 1-μm bands of orthopyroxene and olivine and about 0.035 μm for the 2-μm band in orthopyroxene (Adams 1974)). Note that continuum removed spectra show other shifts depending on the way of continuum choice.

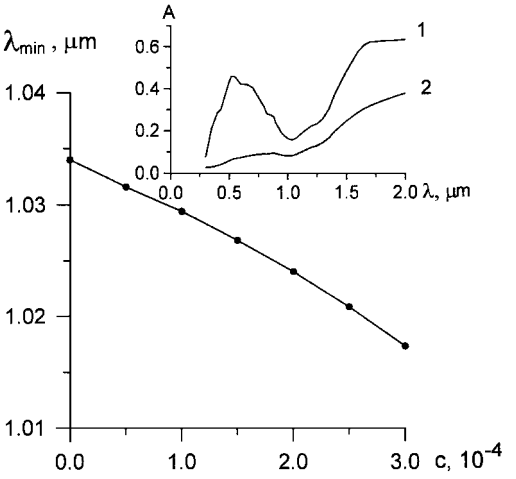

FIG. 11. Dependence of the wavelength positions of the 1-μm band for olivine on the volume concentration of superfine reduced iron (points). (Inset) 1, Olivine spectrum taken for calculations ($c = 0$); 2, the same with reduced iron ($c = 0.0003$).

In Fig. 13 the plot of 1-μm versus 2-μm band positions for orthopyroxene is shown. Concentration of Fe^0 increases from the right top to the left bottom in the whole range of possible Fe^0 volume concentrations (from 0 to 0.25 vol%, which is about the greatest observed in lunar soils (Morris 1976)). The plot resembles the low Fe part of the Adams (1974) diagram. Thus, in analyzing the band minimum positions in the reflectance spectra

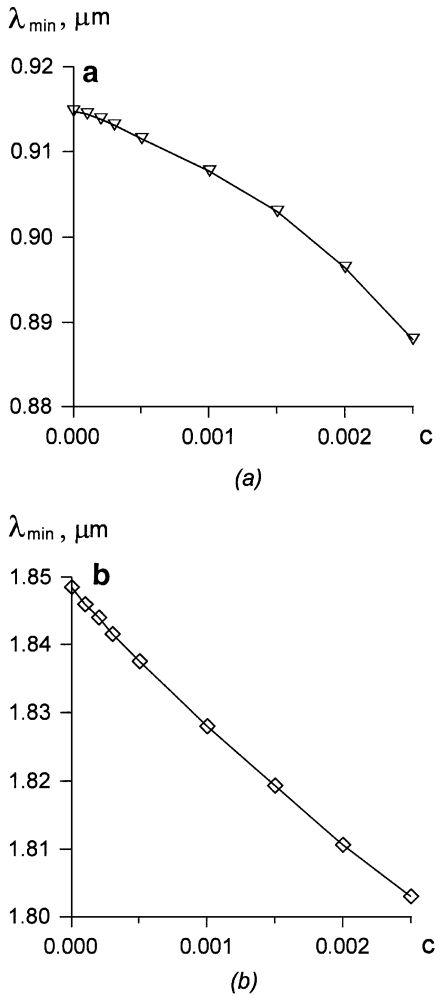

FIG. 12. Calculated positions of the 1-μm (a) and 2-μm (b) bands of orthopyroxene versus volume concentration of superfine reduced iron. (Inset) 1, Pyroxene spectrum taken for calculations ($c = 0$); 2, the same with reduced iron ($c = 0.001$).

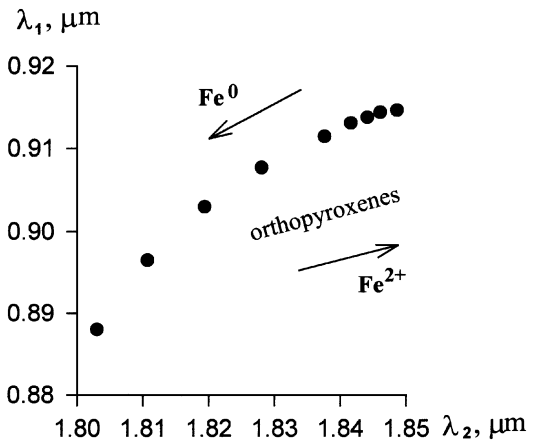

FIG. 13. Calculated plot of the 1-μm versus 2-μm band positions for orthopyroxene influenced by the presence of superfine reduced iron. The iron volume concentration increases from the right to the left.

of iron bearing materials, reduced iron must be taken into account, since it can affect the result of the total Fe content determination and pyroxene type classification on the surfaces of atmosphereless celestial bodies.

CONCLUSIONS

We have developed a simple geometrical-optics model of spectral albedo of powdered surfaces. The model is applicable to surfaces of different structure and composition and uses spectra of optical constants of the components of the surface material. As distinct from the others, our model includes dependence on porosity. Our model is analytically invertible; i.e., explicit formulas are derived to calculate the imaginary part of the refractive index using albedo value, if some *a priori* information about the real part of the refractive index and surface porosity is used.

We applied the model to characterize some physical properties of the lunar regolith. In particular, the following was shown that:

(1) depth of absorption bands for regolith-like surfaces depend on particle size, this is important for interpretation of spectral measurements, especially in search for correlations between the optical characteristics and the abundance of chromofore elements;

(2) when using the 1- and 2-μm band minimum positions for classification of mafic materials by the Adams method, the reduced iron effect should be taken into account.

REFERENCES

Adams, J. B. 1974. Visible and near-infrared diffuse reflectance spectra of pyroxenes as applied to remote sensing of solid objects in the Solar System. *J. Geophys. Res.* **79**, 4829–4836.

Adams, J., and A. Filice 1967. Spectral reflectance 0.4 to 2.0 microns of silicate rock powders. *J. Geophys. Res.* **72**, 5705–5715.

Bodo, Z. 1951. Some optical properties of luminescent powders. *Acta Physica Acad. Sci. Hungarical.* **1** (Fasc. 2), 135–150.

Bohren, C. F., and D. R. Huffman 1983. *Absorption and Scattering of Light by Small Particles.* Wiley, New York.

Carver, J. H., B. H. Horton, D. G. McCoy, *et al.* 1975. Comparison of lunar ultraviolet reflection with that of terrestrial rock samples. *The Moon* **12**, 91–100.

Charette, M. P., T. B. McCord, C. M. Pieters, and J. B. Adams 1974. Application of remote spectral reflectance measurements to lunar geology, classification and determination of titanium content of lunar soils. *J. Geophys. Res.* **79**, 1605–1613.

Cloutis, E. M., M. J. Gaffey, T. Jackowski, and K. Reed 1986. Calibration of phase abundance, composition, and particle size distribution for olivine-orthopyroxene mixtures from reflectance spectra. *J. Geophys. Res.* **91**, 11641–11653.

Dement'ev, B. D., and M. N. Markov 1978. Infrared emission and Lunar spectroscopy. *Tr. Fis. Inst. Acad. Sci. USSR* No 105, 169–203.

Dikov, Yu. P., O. A. Bogatikov, V. L. Barsukov, *et al.* 1978. Some features of the main element conditions in surface layers of the regolith particles of the "Luna" automatic stations samples: X-ray photoelectric spectroscopy studies. *Proc. Lunar Sci. Conf. 9th*, 2111–2124.

Domingue, D., and B. Hapke 1989. Fitting theoretical photometric functions to asteroid phase curves. *Icarus* **78**, 330–336.

Gold, T., E. Bilson, and R. L. Baron 1975. Auger analysis of the lunar soil: Study of processes which change the surface chemistry and albedo. *Proc. Lunar Sci. Conf. 6th*, 3285–3303.

Hapke, B. W. 1981. Bidirectional reflectance spectroscopy. I. Theory. *J. Geophys. Res.* **86**, 3039–3054.

Hapke, B. W. 1984. Bidirectional reflectance spectroscopy. 3. Correction for macroscopic roughness. *Icarus* **59**, 41–59.

Hapke, B. W. 1986. Bidirectional reflectance spectroscopy. 4. The extinction coefficient and the opposition effect. *Icarus* **67**, 264–280.

Hapke, B. W., and E. N. Wells 1981. Bidirectional reflectance spectroscopy. 2. Experiments and observations. *J. Geophys. Res.* **86**, 3055–3060.

Hapke, B., W. Cassidy, and E. Wells 1975. Effect of vapor-phase deposition processes on the optical, chemical, and magnetic properties of the lunar regolith. *The Moon* **13**, 339–353.

Henry, R. C., W. M. Fastie, R. L. Lucke, and B. W. Hapke 1976. A far-ultraviolet photometer for planetary surface analysis. *The Moon* **15**, 51–65.

Hiroi, T., and C. Pieters 1992. Effect of grain size and shape in modelling reflectance spectra of mineral mixture. *Proc. Lunar Planet. Sci. Conf. 22nd*, 313–325.

Johnson, P. B., and R. W. Cristy 1974. Optical constants of metals: Ti, V, Cr, Mn, Fe, Co, Ni, and Pd. *Phys. Rev. B.* **9**, 5056–5070.

Lamy, P. I. 1978. Optical properties of silicates in far ultraviolet. *Icarus* **34**, 68–75.

Lucey, P., G. Taylor, and E. Malaret 1995. Abundance and distribution of iron on the Moon. *Science* **268**, 1150–1153.

Lumme, K., and E. Bowell 1981a. Radiative transfer in the surfaces of atmosphereless bodies. I. Theory. *Astronom. J.* **86**(11), 1694–1704.

Lumme, K., and E. Bowell 1981b. Radiative transfer in the surfaces of atmosphereless bodies. II. Interpretation. *Astronom. J.* **86**(11), 1705–1721.

Melamed, N. 1963. Optical properties of powders. *J. Appl. Phys.* **34**, 560–570.

Morris, R. V. 1976. Surface exposure indices of lunar soils: A comparative FMR study. *Proc. Lunar Sci. Conf. 7th*, 315–335.

Morris, R. V. 1977. Origin and evolution of the grain-size dependence of the concentration of fine-gained metal in lunar soils: The maturation of lunar soils to a steady-state stage. *Proc. Lunar Sci. Conf. 8th*, 3719–3747.

Pieters, C. 1978. Mare basalt types on the front side of the Moon: A summary of spectral reflectance data. *Proc. Lunar Sci. Conf. 9th*, 2825–2849.

Pieters, C., O. Rode, E. Fischer, and A. Basu 1993. Optical effects of space weathering: The role of the finest fraction. *J. Geophys. Res.* **98**(E11), 20817–20824.

Pollack, J. B., O. B. Toon, and B. N. Khare 1973. Optical properties of some terrestrial rocks and glasses. *Icarus* **19**, 372–389.

Rosenberg, G. V. 1967. Physical principles of spectroscopy of light-scattering substances. *Usp. Fiz. Nauk* **91**(4), 569–608.

Simons, E. L. 1975. Diffuse reflectance spectroscopy: Comparison of the theories. *Appl. Opt.* **14**(6), 1380–1386.

Shkuratov, Yu. G. 1982. Albedo of the Moon. *Vestn. Khark. Univ.* **17**, 22–31.

Shkuratov, Yu. G. 1987. A model of spectral albedo dependence for solid surface of cosmic bodies. *Kinemat. Fiz. Nebesnykh Tel* **3**, 39–46.

Shkuratov, Yu. G., D. G. Stankevich, V. G. Kaydash, and N. V. Bondaranko 1997. The relationship between albedo and color-index of the Moon. *Astron. Vestn.* **31**, 46–55.

Starukhina, L. V., and Yu. G. Shkuratov 1996. A model for spectral dependence of albedo for multicomponent regolith-like surfaces. *Astron. Vestn.* **30**(4), 299–306.

Starukhina, L. V., Yu. G. Shkuratov, O. D. Rode, and C. M. Pieters 1994. Reflectance spectra of particle size separates of lunar soils: Is the difference controlled by reduced iron? *Lunar Planet Sci. 25th*, 1333–1334.

Stokes, G. G. 1904. On the intensity of the light reflected from or transmitted through a pile of plates. *Math. Phys. Papers* **4**, 145–156.

Wu, H. H., and A. L. Broadfoot 1977. The extreme ultraviolet albedos of the planet Mercury and of the Moon. *J. Geophys. Res.* **82**, 5.